2012

Dominant Flow Mechanisms in Falling-Film and Droplet Mode Evaporation Over Horizontal Rectangular Tube Banks

John G. Bustamante
sgarimella@gatech.edu

Srinivas Garimella

Dominant Flow Mechanisms in Falling-Film and Droplet Mode Evaporation over Horizontal Rectangular Tube Banks

John G. Bustamante[1], Srinivas Garimella[2]*

[1]Sustainable Thermal Systems Laboratory
George W. Woodruff School of Mechanical Engineering
Georgia Institute of Technology
Atlanta, GA 30332
(404) 385-7288; john.bustamante@gatech.edu

[2]Sustainable Thermal Systems Laboratory
George W. Woodruff School of Mechanical Engineering
Georgia Institute of Technology
Atlanta, GA 30332
(404) 894-7479; sgarimella@gatech.edu

* Corresponding Author

ABSTRACT

Flow visualization with high-speed video of evaporating water films falling over flat horizontal tubes, representative of the external surfaces of microchannel tubes, is presented. Experiments were conducted with 1.4 mm thick and 27 mm tall tubes over a film Reynolds number range of $23 < Re < 126$. In addition to a qualitative description of the flow mechanisms, this work quantifies key droplet and wave characteristics using image analysis techniques. A semi-autonomous edge-detection technique is used to develop a mathematical description of the droplets and waves, allowing the surface area, volume, velocity, and frequency of the droplets, as well as the width, surface area, and velocity of the waves, to be measured. The results are useful for developing accurate, phenomena-based models for falling-film evaporation over flat horizontal tube banks.

1. INTRODUCTION

Falling-film evaporators have applications in refrigeration, desalination, and other areas. They have several advantages over flooded evaporators: a lower refrigerant charge, minimal pressure drop, and operation over small temperature differences. Several possible configurations for falling-film evaporators, based primarily on films falling over horizontal or vertical round tubes, have been investigated. However, one promising geometry that has received little attention is the use of flat microchannel tubes. Microchannel tubes have a thin, rectangular profile with a series of small internal ports, each with a hydraulic diameter on the order of 1 mm, allowing fluid flow in the lengthwise direction. In an evaporator utilizing microchannel tubes, the tubes could be orientated horizontally in a vertical array with in-tube cooling and an external evaporating thin film. These microchannel tubes possess several characteristics that make them ideal for such a configuration: high surface area-to-volume ratios for the internal and external flows, the ability to withstand high internal pressures, and a low refrigerant charge. The usage of external falling-film evaporation over the microchannel tubes is expected to provide high heat transfer coefficients by enhancing thin film heat transfer on a vertical surface with droplet-induced waves. Combining this flow mode with internal cooling will provide very high overall heat transfer coefficients.

There is very little information available in the literature on falling films over rectangular horizontal tubes. However, falling-film evaporation over horizontal round tubes has received considerable attention. A horizontal-tube falling-film type evaporator was first patented in 1888 (Ribatski and Jacobi, 2005), but the topic received little attention until the 1970s, when Chun and Seban (1971, 1972) measured heat transfer coefficients for evaporating water films on vertical tubes, and developed correlations for the laminar, wavy-laminar, and turbulent regimes. Then, Fletcher *et al.* (1974; 1975) examined the heat transfer coefficients for evaporation of water and sea water films from horizontal tubes with plain and knurled surfaces. Chyu and Bergles (1987) conducted additional experiments on water evaporating from plain tubes and introduced a segmented model for prediction of heat transfer

coefficients that divided the flow into the jet impingement, thermally developing, and fully developed regions. Chen and Kocamustafaogullari (1989) experimentally and numerically demonstrated the potential of coupling external falling-film evaporation with internal steam condensation, achieving overall heat transfer coefficients of the order of 3 kW/m^2-K. Falling-film evaporation continued to be examined experimentally, with Parken *et al.* (1990) examining boiling and nonboiling falling films on horizontal smooth tubes and developing empirical correlations for heat transfer coefficients under both conditions, and Fujita and Tsutsui (1998) conducting tests with R11, and studying the impact of dryout on heat transfer. These investigations have continued, with several recent studies providing heat transfer coefficients over wider operating ranges and examining key issues such as dryout. These include a study by Roques and Thome (2007a, b) on boiling of R134a falling films over 4 types of tubes, and experiments by Li *et al.* (2011a; 2011b) on falling-film evaporation of water at 1000 Pa with smooth and enhanced tubes, using the low pressure to eliminate nucleate boiling and only allow convection evaporation. A more thorough review of the experimental and modeling efforts in these areas can be found in the reviews by Thome (1999), Ribatski and Jacobi (2005), and Mitrovic (2005). These experiments have provided significant data on the heat transfer coefficients for a wide range of fluids, flow rates, geometries, and tube surfaces. In addition, insight has been gained into flow mode transitions, wave characteristics, dryout, and other key mechanisms. To the authors' knowledge, only Wang *et al.* (2010, 2011) have studied falling-films over similar rectangular tube geometries. Their initial work (Wang *et al.*, 2010) focused on the flow modes and transitions of water and ethylene glycol in adiabatic conditions with no vapor flow over tubes with a height of 25.4 mm and width of 3.18 mm, and recognized the potential for a microchannel evaporator with in-tube condensation and external evaporation. They observed flow modes similar to those observed between horizontal tubes: sheet, sheet-jet, jet, jet-droplet, and droplet. In addition, they noted several potential differences between round and flat tubes, including the possibility that the Taylor instabilities known to determine the spacing between droplet departure sites will not be as significant on flat tubes, and that different gravitational and shear force distributions could result in new velocity profiles, leading to new flow patterns. A second study (Wang *et al.*, 2011) explored the local and average sensible heat transfer coefficients for falling-films on horizontal flat tubes for a range of heat fluxes, tube spacings, and flow rates. They found that the average Nusselt numbers for flat tubes are similar to those for round tubes in the droplet mode, but are approximately double those of round tubes in the jet and sheet flow modes.

In addition to these studies, investigations focusing on droplet formation, break-up, and impact, which have been studied extensively, are relevant to the current work. A review by Eggers (1997) discusses many of the experimental, analytical, and computational approaches used to understand droplet behavior. Reviews by Rein (1993) and Yarin (2006) provide further information on droplet impacts on dry walls, liquid pools, and thin films. In addition to these general studies, several investigations have focused specifically on aspects of droplet behavior relevant to evaporating falling films. Yung *et al.* (1980) investigated the droplet spacing, droplet diameter, and droplet deflection due to crossflow in falling-film evaporators with horizontal round tubes, and established conditions under which these considerations are important. More recently, Killion and Garimella (2003) used high-speed video to identify deviations from the idealized film behavior often assumed in horizontal tube falling-film models. These characteristics included development of droplet formation sites, the progression of shapes during droplet development, the formation, stretching, and breakup of the liquid bridge, satellite droplets, waves, and interaction between each mechanism. They later extended this analysis with an investigation of aqueous lithium-bromide falling-films over horizontal tubes with an outer diameter of 15.9 mm (Killion and Garimella, 2004a, b). A semi-automated edge-detection program was used to identify the droplets, and calculate their surface area and volume during formation, detachment, fall, and impact. These experiments were conducted to aid in the development of more realistic heat and mass transfer models for absorbers in absorption heat pumps.

It is clear from the above discussion that there has been very little investigation of falling-films on rectangular horizontal tubes. Falling films over round tubes have been studied extensively, but investigations of films falling over rectangular tubes have been limited to studies of adiabatic flow transitions and single-phase heat transfer. There have been no studies examining falling-film evaporation on this microchannel tube geometry, and there is a need for investigation of flow characteristics and heat transfer coefficients with this configuration. The present study, therefore, qualitatively and quantitatively examines droplet and wave characteristics of falling-film evaporation on rectangular horizontal tubes in the droplet flow mode using high-speed video. Water at saturated conditions is used as a working fluid, and flows over heated, flat tubes with a height of 27.4 mm and width of 1.4 mm. Key flow characteristics are quantified using an image analysis program based on the techniques developed by Killion and Garimella (2004a) to examine droplets from horizontal tubes during absorption. The image analysis program collects data on the width, surface area, volume, velocity, and frequency of droplets at the time of impact, as well as

wave width, velocity, and surface area. This information will be useful for the development of heat transfer models for this geometry.

2. EXPERIMENTAL APPROACH

A test facility was developed to enable measurement of heat transfer, and simultaneous flow visualization of evaporating films falling over flat horizontal tubes at sub-atmospheric pressures. A schematic and photograph of this test facility are seen in Figure 1. It includes a primary flow loop for the refrigerant, a vacuum chamber holding the test section, a secondary flow loop for temperature and pressure control, and appropriate instrumentation.

In the main refrigerant flow loop, saturated liquid exits the test chamber and flows down to a magnetic gear pump, which sets the flow rate of the refrigerant. It then flows through a heat exchanger coupled to chilled water lines, bringing the liquid to a subcooled condition. The flow rate is read with a positive displacement flow meter, and an electric heater brings the flow to within 0.2°C of saturated conditions before entering the test chamber. The test chamber is a cubic anodized aluminum vacuum chamber with internal dimensions of 0.61 × 0.61 × 0.61 m. The front surface of the chamber is made of transparent acrylic, allowing full visual access to the test section. In addition, there is a 0.33 m square acrylic window on the back of the test chamber, providing additional area to supply lighting for high-speed video. Within the chamber, the fluid enters the liquid distributor and flows over a vertical array of four horizontal rectangular tubes. The top tube is adiabatic and aids in providing liquid distribution representative of that in an array of flat tubes. The remaining tubes are heated, evaporating some of the test fluid. The evaporated test fluid is condensed by two cold plates at the top of the test chamber, allowing a constant pressure to be maintained in the test chamber. The liquid from these cold plates, as well as fluid that does not evaporate while flowing over the heated tubes, flows to the bottom of the chamber, where a constant liquid level is maintained to supply a consistent gravitational head on the pump.

The liquid distributor is a stainless steel and Plexiglas rectangular box with dimensions of 254 × 31 × 83 mm (length × width × height). The liquid enters from a tube above the center of the distributor, and exits through an array of small vertical tubes centered on the bottom plate of the distributor. Each vertical tube has an inner diameter of 0.83 mm, an outer diameter of 1.27 mm, and a height of 16 mm, evenly distributed above and below the bottom plate of the distributor. The tubes have a center-to-center distance of 4.75 mm, with a total liquid distribution length of 203 mm. The small vertical tubes help ensure good lateral distribution of the test fluid by providing evenly spaced sites with an even pressure head.

The test section shown in Figure 2 is constructed of aluminum with external dimensions of 203 × 1.42 × 27.4 mm (length × width × height) and rounded edges lengthwise. Internally, it contains a polyimide film electric heater and

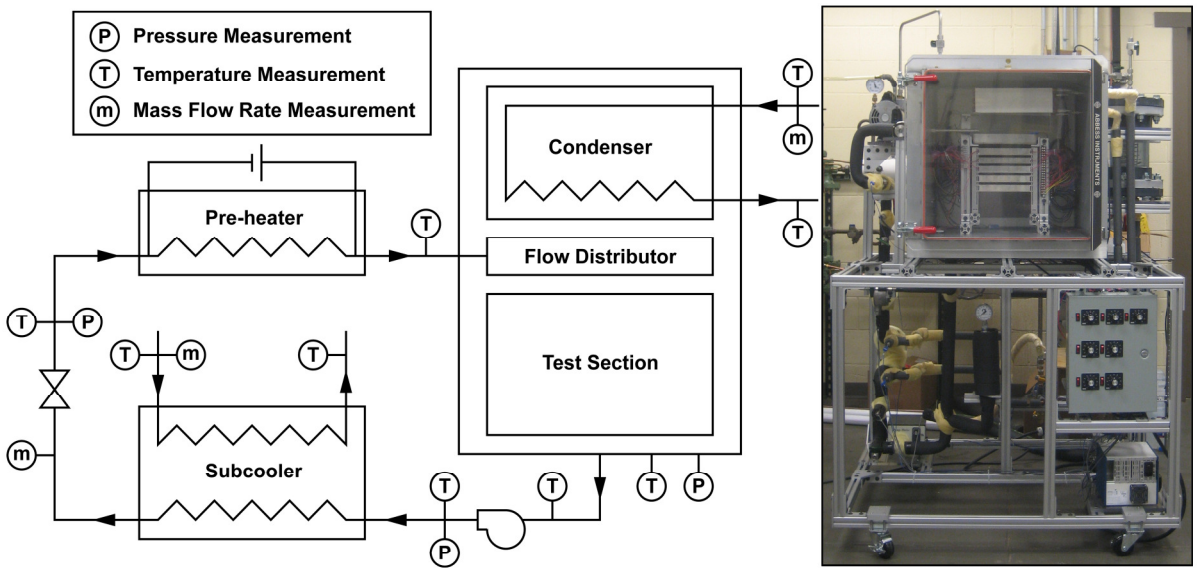

Figure 1: Schematic and picture of the test facility. Valves, fittings, and auxiliary components are not shown in the schematic for clarity.

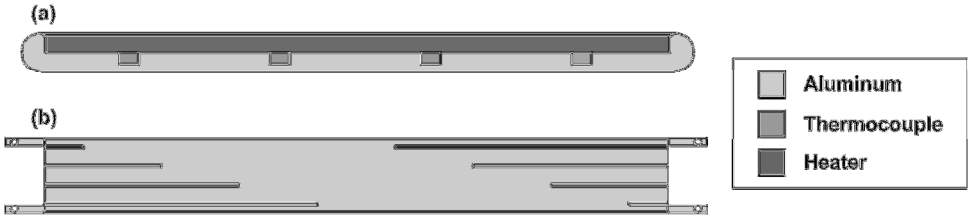

Figure 2: Electrically heated test section: (a) zoomed side view of assembled tube, and (b) front view of machined aluminum piece.

eight 40 gauge thermocouples arranged in two diagonal lines across the tube, offset at the midpoint from one another. It is connected to a mounting stand with four small extensions with a height of 3.9 mm each to limit the heat loss due to conduction. The test section is constructed of a machined aluminum plate with features cut out for the heater and thermocouples, and covered with a 0.25 mm thick aluminum shim to ensure a uniform outer surface. The thermocouples are soldered in place to minimize thermal contact resistance, and the remaining parts are bonded with high thermal conductivity cement. The wide, shallow groove for the electric heater and aluminum shim is 0.71 mm deep, allowing room for both components and two thin layers of bonding cement. The thermocouple grooves are each 0.66 mm wide and 0.46 mm deep, and space the thermocouples 25.4 mm apart axially and 5.7 mm apart vertically. This results in the aforementioned even thermocouple spacing across the tube in two diagonal lines. Before testing, the surface is polished with emery cloth 320/P400 to provide a uniform surface finish and enhance wetting.

T-type thermocouples were used in the test sections and flow loop. Each was individually calibrated in the applicable range by reference to measurements made with a precision NIST-traceable RTD with an accuracy of ±0.05 K, resulting in the uncertainties of most thermocouples being less than ±0.10 K, with some up to ±0.20 K. The pressure within the vacuum chamber was read by a high accuracy pressure transducer with a range of 0 to 34 kPa absolute and an accuracy of ±0.08% of full scale, providing an absolute uncertainty of ±28 Pa. The flow rate in the primary flow loop is measured by a positive displacement flow meter with an accuracy of ±0.5% of reading. The flow rate of the chilled water lines is measured with a series of rotameters accurate to within ±2%.

A high-speed camera made by Photron was used to take the falling-film images. It has a resolution of 1024 × 1024 at 500 frames per second and with enough internal memory to store 1 s of video. Two 500 W tungsten/halogen bulbs with an illumination temperature of 3200 K were used with appropriate filters to provide enough lighting for the high frame-rates and shutter speeds used.

3. PROGRESSION OF THE INTERFACE

The flow patterns over rectangular horizontal tubes are similar to those over horizontal round tubes, which were described in detail by Killion and Garimella (2003). A brief description is presented here. Figure 3 shows a typical droplet formation, droplet impact, and wave formation from an undisturbed portion of the film. The initial disturbance in the film is caused by film instabilities and is stretched in the axial tube direction. A droplet then begins to form as more fluid arrives (Figure 3, frames a-e), a process that is often significantly accelerated by the arrival of a wave. As the droplet grows, it elongates downward due to gravitational forces and develops a spherical cap (Figure 3, frames f-h). The droplet continues to stretch further and a narrow liquid neck is formed between the droplet and the tube (Figure 3, frames i-l). For the geometry under consideration, this liquid neck usually still connects the droplet to the tube when the droplet impacts the next tube. As the droplet forms a wave and begins flowing over the next tube, this liquid bridge between the two tubes breaks up. During breakup the liquid inventory in this bridge is split into three parts: a portion that joins the droplet and flows over the tube below, the volume that is retracted into the film of the originating tube, and the liquid that forms small satellite droplets between the tubes (Figure 3, frames n-q). Each impacting droplet initiates a wave on the tube below. This wave assumes the saddle shape characteristic of flow over round tubes, and is elongated down the tube (Figure 3, frames m-r). These waves travel down the tube in the form of roll waves. A thin film is maintained both upstream and downstream of the wave except in areas of dryout, which can cover a significant portion of the tube at low flow rates.

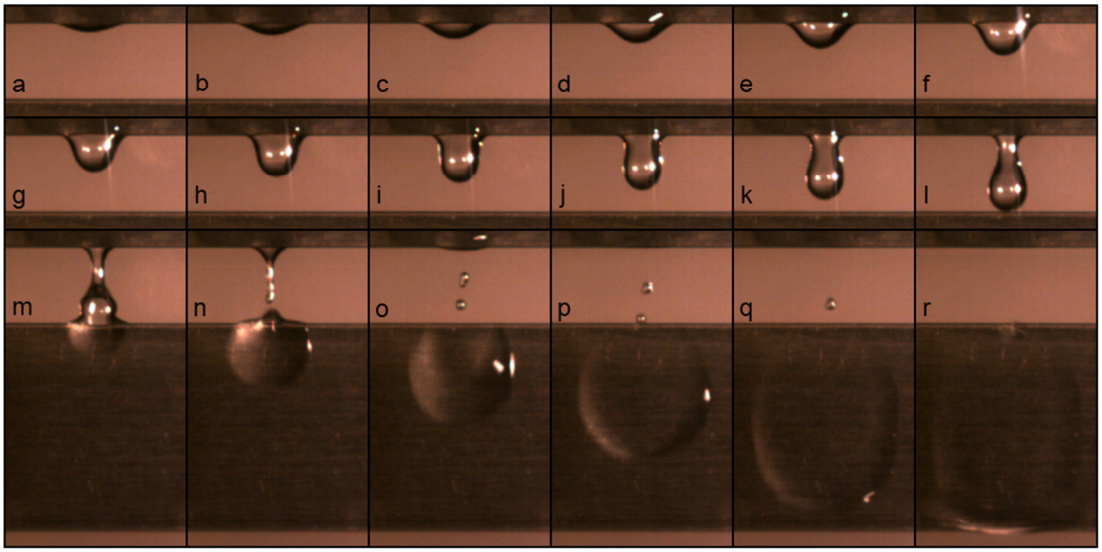

Figure 3: Progression of a pendant drop and wave (a-g: 20 ms between frames, g-r: 10 ms between frames).

This droplet and wave development pattern is relatively consistent when it is not disturbed by other phenomena, but in many cases interactions between droplets, waves, and dryout impact the structure and patterns of each phenomenon. This results in many droplets not having a pendant shape, and waves not assuming a saddle profile. In addition, these interactions change the velocity and size of the droplet or wave. For instance, a wave arrival during droplet formation can significantly accelerate droplet formation. Such interactions are frequent occurrences, particularly at high flow rates. The possible behaviors resulting from these interactions are similar to those in flow over round tubes, which were documented by Killion and Garimella (2003). They are not examined in detail here.

4. IMAGE ANALYSIS

The video frames described above were also analyzed mathematically to extract quantitative information on key droplet and wave characteristics. The selected image analysis method is based on the techniques developed by Killion and Garimella (2004a) to examine evolving films and droplets on horizontal tube banks. Using a semi-automated process, the edges of the droplets and waves are identified and fit with splines. These splines, with appropriate geometric assumptions, are then used to determine the droplet frequency, droplet width, droplet surface area, droplet volume, droplet velocity, wave width, wave velocity, and wave surface area.

The image analysis method is semi-autonomous, and begins with the user manually identifying the droplet or wave to be analyzed. Then, the edge of the droplet or wave is detected and fit with a spline. This spline allows the quantities of interest to be determined. A brief description of each of these steps is provided below, and a more detailed explanation can be found in the work by Killion and Garimella (2004a). The entire process is carried out using a program written in the commercial software program MATLAB (Mathworks, 2010), with a graphical user interface (GUI) that allows the analysis to be performed efficiently on a large number of video frames.

The first step in the method is the manual identification of the location and approximate shape of the droplet or wave to be analyzed. This step is performed manually due to the difficulty of autonomously identifying the relevant edges among all of those typically present in each video frame. These initial selections are used to define a region of interest, within which an appropriate edge-detection algorithm identifies the edges of the droplet or wave. In this case, the Canny edge-detection algorithm (1986) was selected with appropriate thresholds. For situations where the entire interface was not correctly identified with this algorithm, the edge points could be manually moved as needed. This was encountered most frequently with waves, which do not maintain a consistent light gradient along the entire edge of the wave, making it difficult to identify a single set of light intensity thresholds. The second step in the image analysis process is fitting a spline to the previously determined edges. Splines are piecewise polynomial functions that blend smoothly, allowing the identified edges to be combined into a single curve. The spline

algorithms in the MATLAB Spline Toolbox, based on the work of de Boor (1978), were used in this analysis. The final step in the process is using the splines to determine the desired quantities: width, surface area, volume, and velocity. The width and velocity of the waves and droplets can be directly calculated based on measured dimensions. To determine the surface area and volume of the droplets, it was necessary to assume a cross-sectional profile. Pendant droplet profiles are approximately axisymmetric about their vertical axis, so this vertical axis was used as an axis of revolution to create a three-dimensional shape. The average of the two edges was used as the axis of revolution, and each edge was revolved separately, allowing an average value to be used. This profile was integrated numerically using an adaptive Simpson quadrature method to calculate the surface area and volume. The wave surface was also calculated numerically with an assumed flat profile. In other words, the surface area of the wave spline was calculated without accounting for three-dimensional characteristics. Finally, the droplet frequency was tracked independently using a simple marking system with manual inputs.

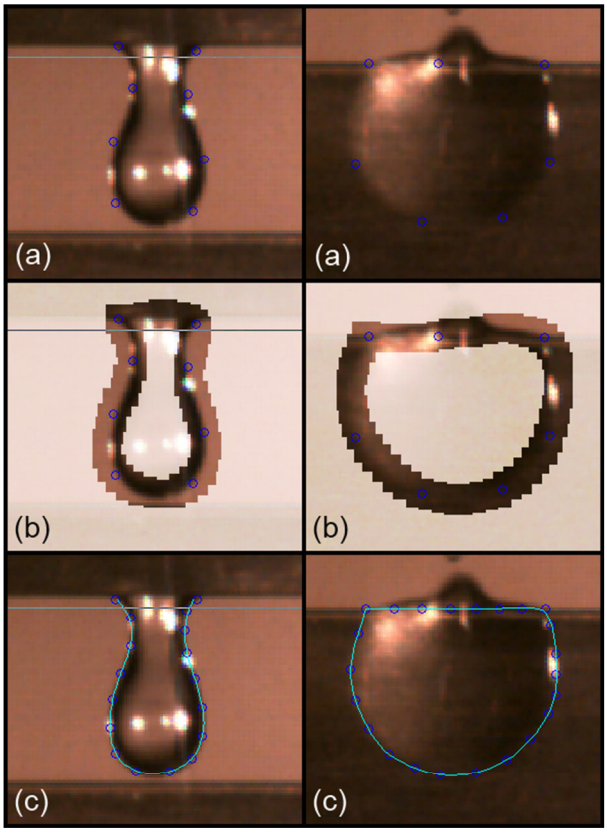

Figure 4: Steps of image analysis: (a) manual selection of interface location, (b) region of interest defined, and (c) edge detected and spline fit.

5. RESULTS

Experiments were conducted over a film Reynolds number range of $23 < Re < 126$ at a saturation temperature of 17°C, corresponding to a saturation pressure of 1940 Pa. This Reynolds number range represents a flow rate range of $0.006 < \Gamma < 0.034$ kg/m-s, where Γ is the flow rate per unit length on one side of the tube. Each tube received 125 W of heat input, resulting in a heat flux of 10.8 kW/m^2. This flow rate range represents the droplet flow regime, bounded by substantial dryout at the low end and the transition to column flow at the high end. Within this range, videos were analyzed at four flow rates corresponding to Re = 23, 57, 92, and 126. Except where noted, four independent videos were analyzed at each flow rate. Each video was taken during separate testing periods, and the system was discharged and recharged between tests. Averages from multiple videos were used to account for the unique flow patterns that develop during different test periods. This is particularly significant at low flow rates, because areas of dryout are not the same for each test. In all figures, Tube 1 refers to the top tube, Tube 2 refers to the middle tube, and Tube 3 refers to the bottom tube.

The droplet frequency results are shown in Figures 5 and 6. In both data sets, only primary droplets are considered. There is no differentiation based on droplet size or formation of temporary liquid bridges, and satellite droplets are not included. Combining the results of the four videos, a total of between 110 and 440 droplet impacts were recorded at each flow rate. As is seen in Figure 5, the droplet frequency increases as flow rate increases. This trend is approximately linear for the top two tubes, but there is a noticeably lower impact frequency for the lowest tube. This suggests that a greater volume of fluid is transmitted by each droplet flowing between Tubes 2 and 3. This can take the form of either larger droplets or more fluid movement through the temporary bridges created by droplets. The

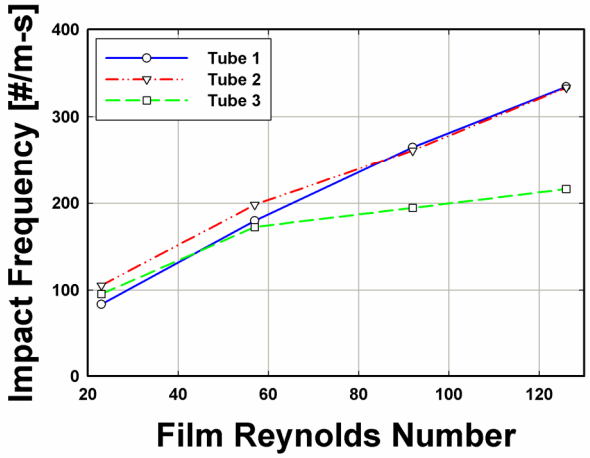

Figure 5: Droplet impact frequency.

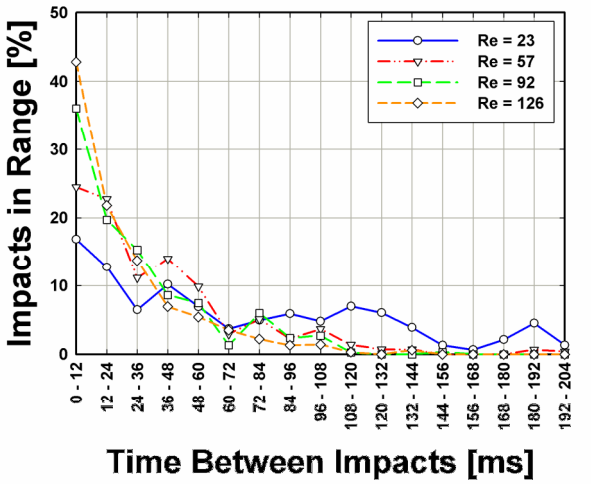

Figure 6: Time between droplet impacts.

volume of the droplets does not increase significantly with flow rate, suggesting that fluid movement through temporary bridges is the dominant influence responsible for this trend. In addition, the time between droplet impacts is shown in Figure 6. The droplet impact distribution appears to be stochastic at all flow rates. This is substantially different from the typical assumptions regarding fluid flow between tubes in falling film models, which often assume either continuous sheet flow or regularly spaced droplets. This droplet impact behavior will in turn affect the heat transfer coefficient of each tube. The timing and number of the droplet impacts will determine the level of waviness and mixing on each tube, and the changing amount of fluid transport through liquid temporary bridges could be a significant factor in tube bundles.

The droplet width, surface area, volume, and velocity at time of impact are shown in Figure 7. Droplets experience a continuous increase in size and velocity up to this moment of impact; therefore, this also represents the maximum of these values during the development of a given droplet. Only pendant droplets were included in the analysis due to limitations of the information captured in the video frames. Because the video was taken only from one side of the tube and not also from the orthogonal axis, features that are not axisymmetric can only be analyzed in a limited fashion. Many irregular droplet shapes were created by interacting phenomena, but are not axisymmetric about the vertical axis and thus would not be accurately captured. For both the surface area and volume measurements, the portion of the droplet within 0.5 mm of the top tube is not included. This cutoff is seen as a horizontal line in Figure 4c and removes the portion of the droplet that is stretched in the axial tube direction. Because this portion of the droplet is not axisymmetric about the vertical axis, the surface area and volume would be overestimated by the image analysis program. The velocity of the droplets is measured from the leading edge of the

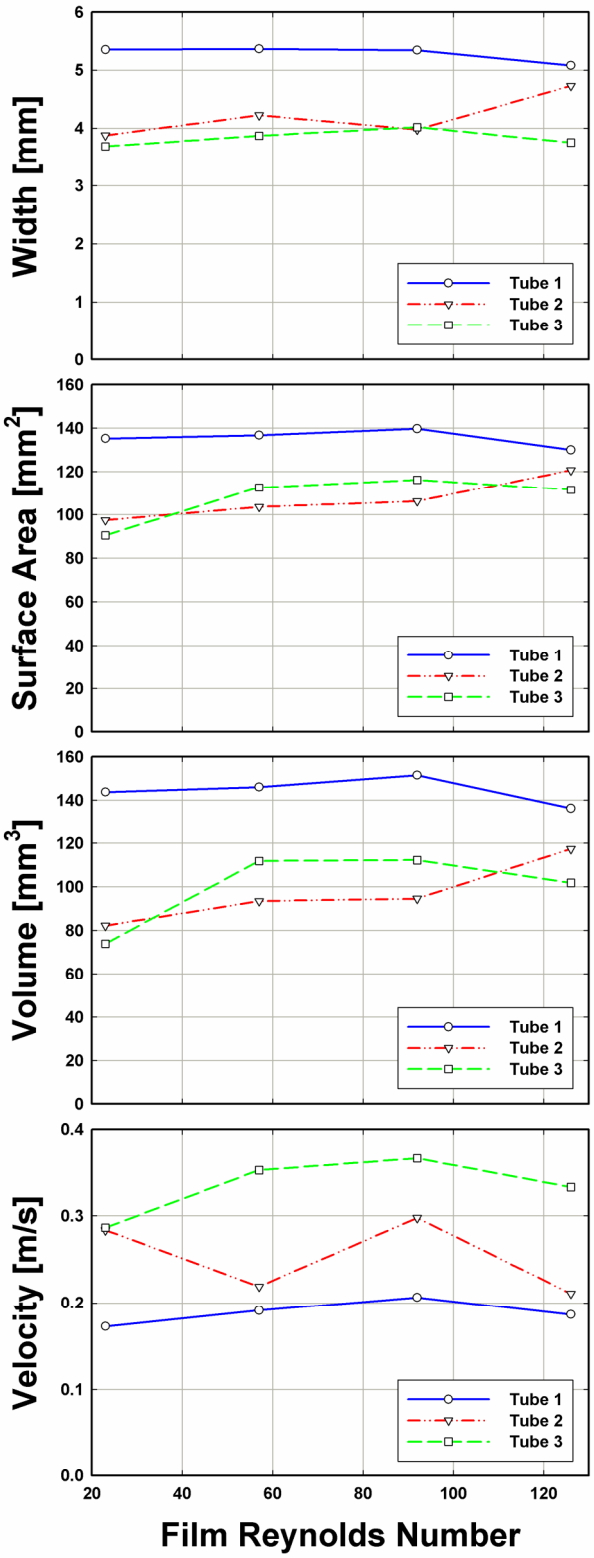

Figure 7: Droplet width, surface area, volume, and velocity.

droplet, and may not be representative of the average velocity of the total droplet. Each data point shown is an average of 15 measurements, taken from the first 5 pendant droplets in 3 videos at the given condition. As is seen in Figure 7, the droplet width, surface area, and volume all exhibit similar trends, and are not significantly influenced by film Reynolds number. Tubes 2 and 3 have similar droplet sizes, but droplets for Tube 1 are substantially larger. This can be attributed to the influence of the liquid distributor. The droplet velocity increases as the tube number increases, but again film Reynolds number has a negligible influence on this parameter.

The wave width, surface area, and velocity are shown in Figure 8. In contrast to the previous data sets, which showed averages of single points across several videos, Figure 8 displays the development of a single wave over time. This is considered more relevant to heat transfer models, as film waviness can significantly enhance heat transfer, and thus the entire wave residence time is important. The wave development is shown from the time of droplet impact to when the wave reaches the bottom of the tube, after which it becomes less distinct and either flows to the bottom of the tube or is absorbed into the film. Three wave developments are shown, all taken at a single flow rate corresponding to Re = 92. The width is measured as the maximum width of the wave, and the velocity is again taken from the leading edge of the wave. The surface area is only that of one side of the tube, and is half of the total surface area resulting from a single droplet if even flow distribution on each side of the tube is assumed. Visually, the waves resulting from droplet impact appeared to be roll waves, which are dominated by gravitational and inertial forces, rather than surface tension. The wave width increases as it flows down the tube, but the width of each wave exhibits a unique trend throughout its development. This may indicate that different amounts of fluid are being supplied by the droplet and liquid bridge providing the liquid for the wave. Despite this, the surface area coverage by each wave exhibits a similar trend, all of which increase throughout the development of the wave. Given that the wave surface area continues to increase after further fluid is no longer being delivered by the droplet and liquid bridge, the average wave thickness must be decreasing, reducing the conductive heat transfer resistance as the wave spreads into a thin film. Meanwhile, the velocity is roughly constant throughout the wave development, with only a slight increase seen in one wave. This is consistent with the expected performance of roll waves, which maintain a relatively constant velocity as they travel down a wall (Patnaik and Perez-Blanco, 1996). Roll waves are characterized by a relatively steep wave front and then smoother slope back to the film thickness after the wave crest. The velocity of the wave will result in a lower convective heat transfer resistance during its passage. In addition, it will mix the fluid from the droplet with the fluid on the tube, replenishing the thin film that is being evaporated by heat transfer from the tube. This aids in avoiding dry spots on the tube, which have a substantially lower heat transfer coefficient.

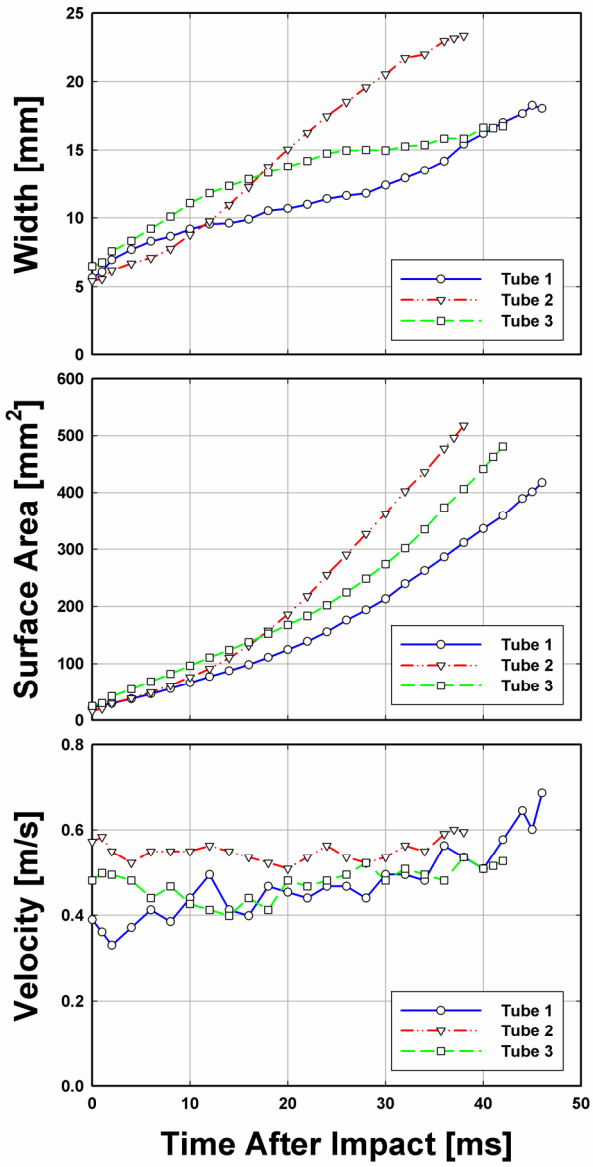

Figure 8: Wave width, surface area, and velocity.

6. CONCLUSIONS

Visualization of evaporating water films falling on horizontal rectangular tube banks allowed flow mechanisms to be examined qualitatively to obtain measurements of key droplet and wave characteristics. In an undisturbed film, pendant droplets form under tubes, impact the tube below, and initiate roll waves that travel down the vertical, flat surface. However, interactions between neighboring droplets and waves can have a substantial impact on the development of each individual droplet and wave. This process shares many similarities with falling-film flow on horizontal round tube banks. A semi-autonomous image analysis method was used to quantify key droplet and wave characteristics. The droplet frequency, width, surface area, volume, and velocity were measured at the time of impact, and wave width, surface area, and volume were tracked during wave development on the vertical flat surface. The droplet frequency increased linearly as flow rate was increased, but the time periods between impacts exhibited stochastic behavior. Droplet width, surface area, volume, and velocity were not influenced significantly by the film Reynolds number, but velocity increased for tubes lower down in the tube bank. The wave width and surface area both increased as the wave developed. Wave velocity remained approximately constant throughout the wave travel. This information is useful for developing accurate, phenomena-based heat transfer models of falling-film evaporation in the film, wave, and droplet regions.

NOMENCLATURE

Re	film Reynolds number, $4\Gamma/\mu$	(–)
Γ	liquid flow rate per unit length on one side of tube	(kg/m-s)
μ	dynamic viscosity	(kg/m-s)

REFERENCES

Boor, C. d., 1978, *A Practical Guide to Splines*. New York, Springer-Verlag, p. 372.

Canny, J., 1986, A Computational Approach to Edge Detection, *Pattern Analysis and Machine Intelligence, IEEE Transactions on*, vol. PAMI-8, no. 6: p. 679-698.

Chen, I. Y. and G. Kocamustafaogullari, 1989, An Experimental Study and Practical Correlations for Overall Heat Transfer Performance of Horizontal Tube Evaporator Design, *National Heat Transfer Conference*, p. 10.

Chun, K. R. and R. A. Seban, 1971, Heat Transfer to Evaporating Liquid Films, *Journal of Heat Transfer*: p. 6.

Chun, K. R. and R. A. Seban, 1972, Performance Prediction of Falling-Film Evaporators, *Journal of Heat Transfer*: p. 5.

Chyu, M.-C. and A. E. Bergles, 1987, An Analytical and Experimental Study of Falling-Film Evaporation on a Horizontal Tube, *Journal of Heat Transfer*, vol. 109: p. 8.

Eggers, J., 1997, Nonlinear Dynamics and Breakup of Free-Surface Flows, *Reviews of Modern Physics*, vol. 69, no. 3: p. 865.

Fletcher, L. S., V. Sernas and L. S. Galowin, 1974, Evaporation from Thin Water Films on Horizontal Tubes, *Industrial & Engineering Chemistry Process Design and Development*, vol. 13, no. 3: p. 265-269.

Fletcher, L. S., V. Sernas and W. H. Parken, 1975, Evaporation Heat Transfer Coefficients for Thin Sea Water Films on Horizontal Tubes, *Industrial & Engineering Chemistry Process Design and Development*, vol. 14, no. 4: p. 411-416.

Fujita, Y. and M. Tsutsui, 1998, Experimental Investigation of Falling Film Evaporation on Horizontal Tubes, *Heat Transfer - Japanese Research*, vol. 27, no. 8: p. 609-618.

Killion, J. D. and S. Garimella, 2003, Gravity-Driven Flow of Liquid Films and Droplets in Horizontal Tube Banks, *International Journal of Refrigeration*, vol. 26, no. 5: p. 516-526.

Killion, J. D. and S. Garimella, 2004a, Pendant Droplet Motion for Absorption on Horizontal Tube Banks, *International Journal of Heat and Mass Transfer*, vol. 47, no. 19-20: p. 4403-4414.

Killion, J. D. and S. Garimella, 2004b, Simulation of Pendant Droplets and Falling Films in Horizontal Tube Absorbers, *Journal of Heat Transfer*, vol. 126, no. 6: p. 1003-1013.

Li, W., X.-Y. Wu, Z. Luo and R. L. Webb, 2011a, Falling Water Film Evaporation on Newly-Designed Enhanced Tube Bundles, *International Journal of Heat and Mass Transfer*, vol. 54, no. 13-14: p. 2990-2997.

Li, W., X.-Y. Wu, Z. Luo, S.-c. Yao and J.-L. Xu, 2011b, Heat Transfer Characteristics of Falling Film Evaporation on Horizontal Tube Arrays, *International Journal of Heat and Mass Transfer*, vol. 54, no. 9-10: p. 1986-1993.

Mathworks, Inc., 2010, Version 7.11.0.584 (R2010b), Natick, Massachusetts.

Mitrovic, J., 2005, Flow Structures of a Liquid Film Falling on Horizontal Tubes, *Chemical Engineering & Technology*, vol. 28, no. 6: p. 684-694.

Parken, W. H., L. S. Fletcher, V. Sernas and J. C. Han, 1990, Heat Transfer through Falling Film Evaporation and Boiling on Horizontal Tubes, *Journal of Heat Transfer*, vol. 112, no. 3: p. 744-750.

Patnaik, V. and H. Perez-Blanco, 1996, Roll Waves in Falling Films: An Approximate Treatment of the Velocity Field, *International Journal of Heat and Fluid Flow*, vol. 17, no. 1: p. 63-70.

Rein, M., 1993, Phenomena of Liquid Drop Impact on Solid and Liquid Surfaces, *Fluid Dynamics Research*, vol. 12, no. 2: p. 61.

Ribatski, G. and A. M. Jacobi, 2005, Falling-Film Evaporation on Horizontal Tubes--a Critical Review, *International Journal of Refrigeration*, vol. 28, no. 5: p. 635-653.

Roques, J.-F. and J. R. Thome, 2007a, Falling Films on Arrays of Horizontal Tubes with R-134a, Part I: Boiling Heat Transfer Results for Four Types of Tubes, *Heat Transfer Engineering*, vol. 28, no. 5: p. 398 - 414.

Roques, J.-F. and J. R. Thome, 2007b, Falling Films on Arrays of Horizontal Tubes with R-134a, Part Ii: Flow Visualization, Onset of Dryout, and Heat Transfer Predictions, *Heat Transfer Engineering*, vol. 28, no. 5: p. 415 - 434.

Thome, J. R., 1999, Falling Film Evaporation: State-of-the-Art Review of Recent Work, *Enhanced Heat Transfer*, vol. 6: p. 263-277.

Wang, X. F., P. S. Hrnjak, S. Elbel, A. M. Jacobi and M. G. He, 2010, Flow Patterns and Mode Transitions for Falling-Films on Flat Tubes, *International Refrigeration and Air Conditioning Conference at Purdue*, Purdue, IL

Wang, X. F., P. S. Hrnjak, S. Elbel, A. M. Jacobi and M. G. He, 2011, Heat Transfer Performance for a Falling-Film on Horizontal Flat Tubes, *ASME 2011 International Mechanical Engineering Congress & Exposition*, Denver, Colorado

Yarin, A. L., 2006, Drop Impact Dynamics: Splashing, Spreading, Receding, Bouncing…, *Annual Review of Fluid Mechanics*, vol. 38, no. 1: p. 159-192.

Yung, D., J. J. Lorenz and E. N. Ganic, 1980, Vapor/Liquid Interaction and Entrainment in Falling Film Evaporators, *Journal of Heat Transfer*, vol. 102, no. 1: p. 20-25.

ACKNOWLEDGEMENTS

The authors gratefully acknowledge the support provided by the U.S. Office of Naval Research under contract number N000140710847 for this research.